Unfreezing Taylor's Hypothesis for Precipitation

J.D. Creutin, E. Leblois, J.M. Lepioufle

Unfreezing Taylor's Hypothesis for Precipitation

J.-D. CREUTIN

Laboratoire d'étude des Transferts en Hydrologie et Environnement, Université Grenoble Alpes and CNRS, Grenoble, France

E. LEBLOIS

Hydrology–Hydraulics Research Unit, Centre de Lyon-Villeurbanne, Irstea, Villeurbanne, France

J.-M. LEPIOUFLE

Norwegian Meteorological Institute, Oslo, Norway

(Manuscript received 27 June 2014, in final form 23 February 2015)

ABSTRACT

Since the seminal work of Zawadzki in the seventies, the so-called Taylor's "frozen" hypothesis has been regularly used to study the statistical properties of rainfall patterns. This hypothesis yields a drastic simplification in terms of symmetry of the space–time structure—the large-scale advection velocity is the conversion factor used to link the time and space autocorrelation functions (ACFs) of the small-scale variability. This study revisits the frozen hypothesis with a geostatistical model. Using analytical developments and numerical simulations tuned on available case studies from the literature, the role of large- and small-scale rainfall kinematics on the properties of the space–time ACF $A(\mathbf{a}, \tau)$ and associated fluctuations is investigated. In particular, the merits and limits of the ACF signature classically used to test the frozen hypothesis are examined. The conclusion is twofold. Taylor's hypothesis, understood as the quest for a space–time symmetry in rain field variability, remains important in hydrometeorology four decades after the pioneering work of Zawadzki. The frozen hypothesis, introduced for simplification purposes, appears difficult to check and too constraining. The methods proposed to check the hypothesis rely too directly on the use of the advection velocity as a space–time conversion factor instead of contemplating the ACF signature more globally. The model proposed that using two characteristic velocities instead of one appears more flexible to fit the ACF behaviors presented in the literature. This remains to be checked over a long-term high-resolution dataset.

1. Introduction

Since the seminal work of Zawadzki (1973), the so-called Taylor's hypothesis has been regularly used to study the statistical properties of rainfall patterns. Various experimental studies used weather radar data to check the validity range of the hypothesis (Crane 1990; Poveda and Zuluaga 2005; Li et al. 2009). Theoretical implications of the hypothesis are considered in several pioneering works, such as in Gupta and Waymire (1987) for space–time models or in Lovejoy and Mandelbrot (1985) for fractals.

The motivation of Taylor (1938) was to find a "space–time conversion factor" extending the time spectrum of turbulence at a point, which was measurable, to a space correlation function at a time and thus to have a time–space model of turbulence. To solve the problem, Taylor considered the turbulent component u_1 parallel to the airstream mean velocity $\mathbf{U}$, and he assumed that this component is negligible as compared to the mean velocity. Physically, $|u_1| \ll \|\mathbf{U}\|$ means that the pattern of turbulence does not change much (low eddy velocities) while moving along the airstream (high advection velocity). When $u_1 = 0$ this led to the idea of a "frozen" field, hence the name of Taylor's frozen hypothesis. In the rest of the paper we will speak about the frozen hypothesis for short, keeping the wording "Taylor's hypothesis" for the more general idea of space–time equivalence of the autocorrelation function (ACF). As seen by a fixed observer, if $A(\mathbf{a}, \tau)$ is the space–time ACF of the 3D space–time stationary random field

Corresponding author address: Etienne Leblois, Irstea-Lyon, 5 rue de la Doua, CS 70077, F-69626 Villeurbanne Cedex, France.
E-mail: etienne.leblois@irstea.fr

DOI: 10.1175/JHM-D-14-0120.1

$R(\mathbf{x}, t)$, the frozen hypothesis leads to the following relationship: $A(\mathbf{0}, \tau) = A(\tau\mathbf{U}, 0)$, which is in substance the Eq. (8) of Taylor (1938) and which expresses a space–time equivalence of the ACF but for a space–time conversion. The specificity of the frozen hypothesis is to take the advection velocity as conversion factor between the time and space ACF. When A is isotropic, the vector $\mathbf{a}$ can be replaced by its norm $\|a\|$.

Zawadzki (1973) transposed this idea to atmospheric precipitation separating de facto two scales of kinematics. The "large scale" movement of precipitation systems is often clearly visible on radar animations and used as such for short-term precipitation forecasting (see, e.g., Austin and Bellon 1974; Bowler et al. 2004). It can be mathematically formulated between instants t_1 and t_2 as $\mathbf{U} = \mathbf{a}_0/(t_1 - t_2)$, where $\mathbf{a}_0$ is the space vector maximizing the ACF $A(\mathbf{a}_0, t_1 - t_2)$. This large-scale movement allows one to distinguish the rainfall variability seen from a coordinate system moving with the storm velocity (Lagrangian perspective) from the variability seen at a fixed set of coordinates (Eulerian perspective). The "small scale" describes the fluctuations of the rain intensity inside the advected precipitation pattern. Germann and Zawadzki (2002) use the two-dimensional conservation equation of the rain intensity R to express in differential form the Eulerian fluctuation of R as the difference between the Lagrangian fluctuation and the advection term following $\partial R/\partial t = dR/dt - \mathbf{U}\partial R/\partial \mathbf{x}$, the frozen hypothesis corresponding to $dR/dt = 0$.

Some studies gave a conceptual interpretation to this transposition of a model of turbulence to precipitation. Gupta and Waymire (1987), referring to their theoretical model for mesoscale rainfall (Waymire et al. 1984), interpreted the cutoff in the hypothesis around 40 km, demonstrated by Zawadzki (1973). Using the "cell" and "cluster" terminology shared by several authors since Austin and Houze (1972), they concluded that the cutoff parameter in the frozen hypothesis is the mean cell life α^{-1} or dissipation time scale, which is much smaller than the mean cluster life β^{-1}. For Crane (1990), the transposition amounts to considering the updraft precipitation generating regions organized at the mesoscale as passive scalars advected by a 2D turbulent flow, the nearest neighbor distance between cells (12 km according to this author) being governed by buoyancy waves excited by convection that in turn trigger new cells. This hypothesis of passive scalars neglects that convection feeds back into the large-scale flow. The advection velocity differs from the mean velocity of a turbulent wind field in the sense that it results from the complex interaction between the precipitation system and its environment through vertical transport of horizontal momentum (see, e.g., Wu and Yanai 1994). In addition, there is no perfect correspondence between convection and precipitation, the differential fall speed of hydrometeors causing them to spread along their fall (Fabry 1996).

Other studies checked the practical adequacy of this model of turbulence to rainfall dynamics. Zawadzki et al. (1994) assessed the predictability of precipitation patterns using Lagrangian persistence, which is the forecasting skill of the frozen hypothesis and which appears to vanish beyond 40–112 min for the radar dataset used. More recently, Poveda and Zuluaga (2005) and Li et al. (2009) used multievent radar datasets to check the frozen hypothesis. With more intense convection and smaller advection velocities than at midlatitude, Amazonian storms exhibit shorter cutoff values (10–15 min) when they satisfy the hypothesis, which is for only 3 storms out of 12 (Poveda and Zuluaga 2005). Two statistical analyses of radar rainfall ACF in the southeastern United States show that the hypothesis does not hold beyond space and time scales resolved by the data [4 km and 15 min, according to Li et al. (2009)].

To our best knowledge, no study questioned the choice of the velocity used to link the space and time ACF. Freezing the small-scale variability allows one to use the large-scale advection as the time–space ACF conversion velocity. This drastic simplification is a sufficient condition of space–time isotropy, but it is not a necessary one, as shown here.

This study revisits the question of the conversion velocity using a geostatistical model that relaxes by construction the frozen hypothesis (Leblois and Creutin 2013). The model considers that the small-scale variability of the rainfall field respects Taylor's hypothesis of similarity of the space and time ACF through a conversion velocity specific of this scale that Leblois and Creutin (2013) name Taylor's velocity. At this stage, the model simulates stationary, homogeneous rainfall fields with a zero mean velocity. The large-scale advection is given a different characteristic velocity field that merely shifts the small-scale variability respecting incompressibility, like, for instance, the most often used uniform advection. The model represents both intermittency and inner rainfall variability, which are assumed independent and thus can have a priori unrelated dynamics.

Using analytical developments and numerical simulations tuned on available literature case studies, we investigate the role of large- and small-scale rainfall variability on the properties of the space–time autocorrelation function $A(\mathbf{a}, \tau)$. We pay particular attention to the ACF signature used in the analysis proposed by Zawadzki (1973) and by subsequent studies to check the frozen hypothesis. As developed below, we call ACF signature the common plot of, on the one hand, the Eulerian and Lagrangian time ACF and, on the

other hand, the space ACF converted to time dimension using the advection velocity.

Section 2 introduces a theoretical formulation of the space–time ACF showing the role of advection and Taylor's velocities. Section 3 takes an exponential model to illustrate analytically how the ACF signature varies when the ratio u^* between advection and Taylor's velocities [see Eq. (10)] varies. Section 4 presents the simulation of advected mesoscale precipitations and their occurrence (SAMPO) and the protocol of the proposed numerical experiment pivoting around the case study presented by Zawadzki (1973). Section 5 examines the uncertainty of the advection velocity assessment. Sections 6 and 7 show how the respective values of the two characteristic velocities influence the test of the frozen hypothesis in the presence and absence of intermittency. Section 8 draws conclusions.

2. Spatial and temporal structure in Lagrangian and Eulerian reference

In this section, we use successive changes of coordinate systems to analytically relate the time and space structure functions that are used to check the frozen hypothesis.

Let $R(\mathbf{x}_0, z_0)$ denote a 3D isotropic stationary random function, where the subscript zero indicates coordinates in an orthonormal coordinate system; $\mathbf{x}$ is a vector indexing the 2D horizontal subspace; and the scalar z indexes the 1D orthogonal dimension. Its 3D ACF reads

$$A(\mathbf{a}, b) = \rho[R(\mathbf{x}_0, z_0), R(\mathbf{x}_0 + \mathbf{a}, z_0 + b)], \qquad (1)$$

where $\rho[\cdot]$ is the correlation and $\mathbf{a}$ and b are arbitrary displacements.

ACF is taken as a generic term and, with no loss of generality, the results presented in this section apply to any form of structure function, including, for instance, the simple covariance chosen in Zawadzki (1973) or variograms. We consider that the ACF is isotropic, that is, in a simplified way $A(\mathbf{a}, 0) = A(\|\mathbf{a}\|, 0) = A(0, \|\mathbf{a}\|)$.

A first simple transformation of the z axis allows us to introduce the time dimension and to get a Lagrangian rainfall field (super- and subscript L) as follows:

$$R^L(\mathbf{x}_L, t) = R(\mathbf{x}_0/\Lambda, z_0/\Delta) = R(\mathbf{x}_L, tU_T), \qquad (2)$$

where t is the time and Λ and Δ are space and time characteristic dimensions, respectively, of the rainfall field, that is, the integral ranges obtained by the mere integration of the ACF in space and time when they are integrable (Lantuéjoul 2002, chapter 4). The variable U_T is a conversion scalar linking time and space dimensions that we name Taylor's velocity (explanation below) and that can be noted $U_T = \Lambda/\Delta$.

In a second step, this steady rainfall field is advected with a velocity vector $\mathbf{U}$ to give the Eulerian view of the rainfall field (super- and subscript E):

$$R^E(\mathbf{x}_E, t) = R^L(\mathbf{x}_E - \mathbf{U}t, t) = R(\mathbf{x}_E - \mathbf{U}t, tU_T). \qquad (3)$$

The space–time ACF of the Lagrangian and the Eulerian rainfall fields are derived from Eqs. (1)–(3) and can be written as follows:

$$A^L(\|\mathbf{a}\|, \tau) = A(\|\mathbf{a}\|, \tau U_T) \qquad (4)$$

and

$$A^E(\|\mathbf{a}\|, \tau) = A(\|\mathbf{a} - \tau\mathbf{U}\|, \tau U_T), \qquad (5)$$

where τ is an arbitrary time lag.

It is easy to see that the Lagrangian and Eulerian ACFs only differ by the time dimension. As long as the space dimension is considered, all the above ACFs are identical with $A^L(\|\mathbf{a}\|, 0) = A^E(\|\mathbf{a}\|, 0) = A(\|\mathbf{a}\|, 0)$. Depending on the relative values of $\mathbf{U}$ and U_T, different simplifications appear.

When U_T is strictly positive, the Lagrangian ACF A^L follows the property of space–time conversion looked for in Taylor (1938), namely, $A^L(0, \tau) = A^L(\tau\mathbf{U}_T, 0)$, as A is isotropic, hence the name of Taylor's velocity given to U_T in Leblois and Creutin (2013).

When U_T tends toward zero, the advected precipitation pattern is frozen, and thus Eq. (3) reads:

$$R^E(\mathbf{x}_E, t) = R(\mathbf{x}_E - \mathbf{U}t, 0). \qquad (6)$$

The space and time Eulerian ACFs are related as in Eq. (2.17) of Zawadzki (1973):

$$A^E(\tau\|\mathbf{U}\|, 0) = A(\tau\|\mathbf{U}\|, 0) = A^E(0, \tau). \qquad (7)$$

Equation (7) tells that when the field is frozen, Taylor's space–time conversion applies to the Eulerian ACF and the conversion velocity is the norm of the advection velocity $\|\mathbf{U}\|$. The Lagrangian time ACF is constant and equals $A(0, 0)$.

When the advection $\mathbf{U}$ is nil, the Eulerian and Lagrangian ACF are identical and Eq. (7) applies to either A^E or A^L while keeping the same conversion velocity. If Taylor's velocity is also nil, the Eulerian ACF equals $A(0, 0)$, that is, there is no variability at all, a mere mathematical limit.

3. ACF signature in a pure exponential case

In the studies applying the frozen hypothesis, the main graphic representation used to check the validity

of Eq. (7) groups three ACFs in the time dimension: the time Lagrangian $A^L(0, \tau)$ and Eulerian $A^E(0, \tau)$ ACF and a space ACF converted to time scale using the advection velocity $A(0, \tau\|\mathbf{U}\|)$ [see, e.g., Fig. 15 of Zawadzki (1973)]. For short, we call this plot the ACF signature. It is worth noting at this stage that most analyses of the ACF signature ignored the Lagrangian ACF and only focused on the fit between the Eulerian and the space-converted ACF, that is, checking Eq. (7) and commenting on an eventual cutoff time like in Zawadzki (1973).

In this section, we show typical behaviors of the ACF signature when the frozen hypothesis is relaxed. The given illustrations are based on an exponential ACF model:

$$A^E(\mathbf{a}, \tau) = \exp[-\text{dist}(\|\mathbf{a}\|, \tau)] \quad \text{with} \quad \text{dist}\ (\|\mathbf{a}\|, \tau) = \sqrt{\|\mathbf{a} - \tau\mathbf{U}\|^2 + \tau^2 U_T^2}. \tag{8}$$

ACF surfaces representing A and A^L (a fully symmetric cone-like surface and its stretching along an axis, respectively) are simpler than the surface representing A^E. Let us consider in Fig. 1 the surface representing the Eulerian ACF A^E in the exponential case when the advection $\|\mathbf{U}\|$ is chosen to be much greater than (frozen, here taken for $u^* = 10.0$ only for numerical reasons), equal to, or smaller than Taylor's velocity U_T. By construction, on this surface the space ACF is read in the vertical plane including the space axis and the time Eulerian ACF is read in the corresponding time plane. The Lagrangian time ACF is less obvious to read. Using Eqs. (4) and (5), the Lagrangian time ACF can be written as

$$A^L(\|\mathbf{a}\|, \tau) = A^E(\|\mathbf{a} - \tau\mathbf{U}\|, \tau), \tag{9}$$

and thus, the time Lagrangian ACF A^L is at the intersection of the ACF surface with the vertical plane oriented along $(\tau\|\mathbf{U}\|, \tau)$.

Figure 1 shows that the Lagrangian time ACF is by construction above the Eulerian one. At this point, it is useful to note that Lagrangian and Eulerian space coordinates are such that

$$A^L(0, \tau) = A^E(\|\tau\mathbf{U}\|, \tau) = A^E(0, \tau\sqrt{1 + u^{*2}}), \tag{10}$$

where $u^* = \|\mathbf{U}\|/U_T$ is the ratio between advection and Taylor's velocities.

Incidentally, one can notice the difference between the line of the maximum cross correlation between successive time steps (maximization at a constant time interval) and the line of the maximum cross correlation between nearby locations (maximization at a constant space interval). The former, the straight line $y = \|\mathbf{a} - \tau\mathbf{U}\|$, is more commonly used in practice to identify the advection velocity than the latter [see Crane (1990), his Fig. 11]. The latter is also influenced by Taylor's velocity and thus provides a biased estimate of the advection velocity, except in the frozen case. As a more general remark, given the sharpening of ACF surfaces, the methods using maximum correlation to estimate the advection velocity are more likely to work when u^* is high (close to frozen and/or high advection).

Figure 2 displays typical ACF signatures. As stated before, the Eulerian time ACF is always below the Lagrangian one and those two ACFs get closer when the advection velocity diminishes. When u^* increases, we observe a twofold movement of the curves. On the one side, the Lagrangian ACF rises up toward a limit value equal to $A(0, 0)$. On the other side, the spatial ACF converted using the advection velocity falls down to reach the Eulerian ACF, that is, toward the satisfaction of the criterion proposed by Zawadzki (1973). When u^* equals 1, advection and Taylor's velocities are equal, and, in turn, the converted spatial and Lagrangian ACFs are identical. This central case basically separates two signatures according to the respective positions of the Lagrangian and spatial ACFs. The extremes of these two signatures are when the Lagrangian or spatial ACF matches the Eulerian ACF (no-advection and frozen cases, respectively). The examination of a continuous range of variation of u^* using a simple visualization software shows that it is graphically possible to distinguish the transition between these extremes only when $0.4 < u^* < 2.5$.

Real-world data in Zawadzki (1973) and Poveda and Zuluaga (2005) can be compared with the aforementioned signatures. Figure 15 of Zawadzki (1973) is probably close to the ambiguous case $u^* = 1$, when the criterion of Eq. (8) is satisfied and when the Lagrangian ACF is clearly far from the frozen case in spite of a significant advection velocity. Figures 2 and 3 of Poveda and Zuluaga (2005) illustrate the signatures well with u^* below and over 1, respectively, which is consistent with their diagnosis of satisfaction of the frozen hypothesis in their Fig. 3. Notice that, in Fig. 3 of Poveda and Zuluaga (2005), the Lagrangian ACFs are close to the flat limit behavior, which is expected in theory from the frozen case.

As a side remark, we can note that the theoretical identification of the Taylor and advection velocities consists of elementary movements over the A^E surface. Looking, for instance, for a maximum value of $A^E(\|\mathbf{a}_0\|, \tau_0)$ at a chosen τ_0 allows to us estimate (i) the advection velocity $\|\mathbf{U}\| = \|\mathbf{a}_0\|/\tau_0$ and (ii) Taylor's velocity from the ratio between $A^E(\|\mathbf{a}_0\|, \tau_0)$ and $A^E(0, \tau_0)$.

In practice, the analysis of experimental rainfall ACF in order to test the frozen hypothesis meets several sources of difficulties, namely, the skewness of the

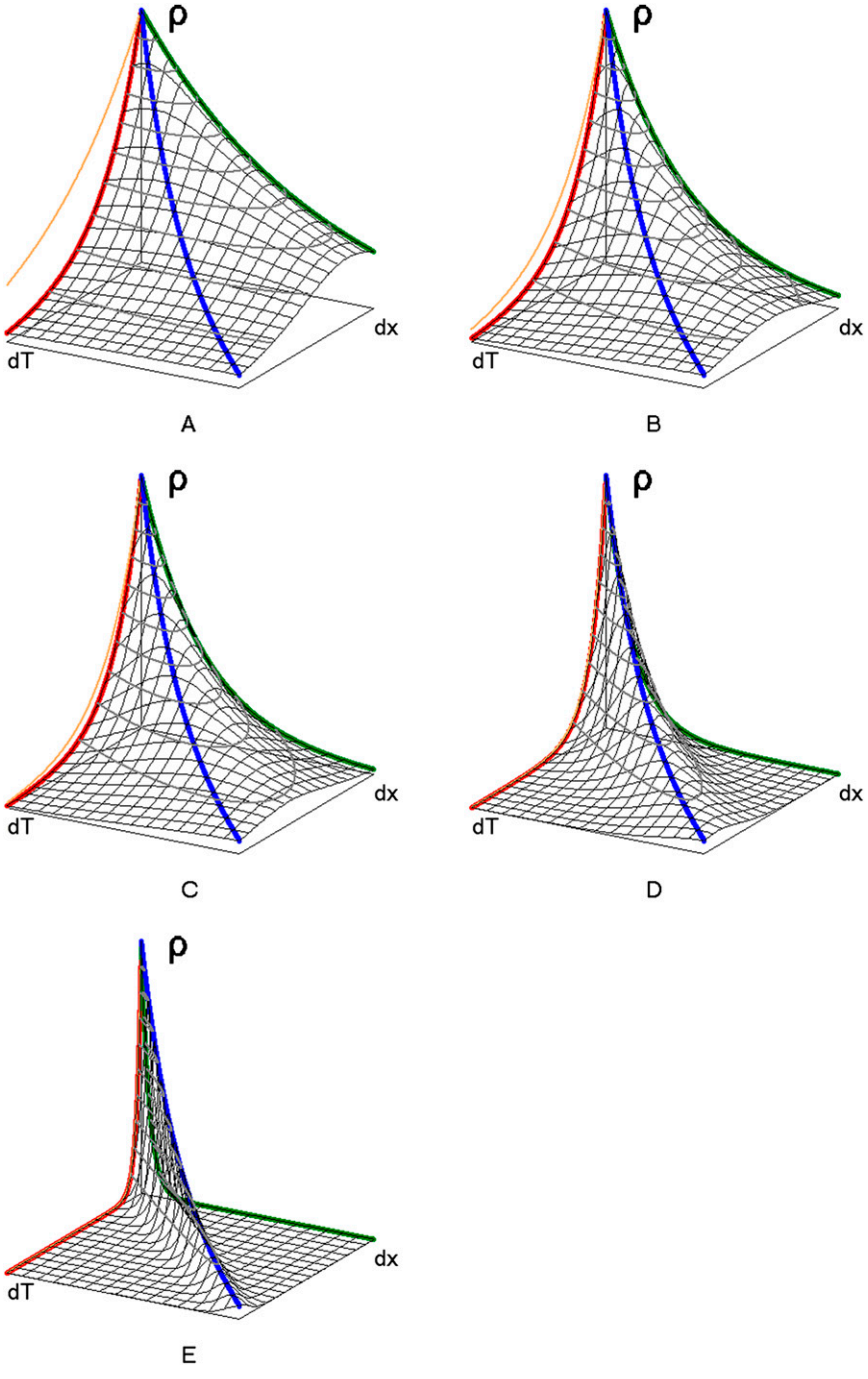

FIG. 1. Three-dimensional Eulerian ACF in space and time. Left axis is the time dimension, and the intersect of the corresponding vertical plane with the Eulerian ACF surface is the time Eulerian ACF (red). Right axis is the space dimension, and the intersect is the space ACF (green). The Lagrangian ACF (blue) is obtained by maximizing the correlation value along a section of the surface at constant time. Given the model used, the crest of max values of correlation for the Lagrangian ACF appears to be a line. The space ACF converted into time dimension with the advection velocity is represented in the time plane (orange). (a)–(e) Correspond to increasing u^* values of 0.5 (close to "static", i.e., weak advection), 1.0, 1.4, 3.0, and 10.0 (close to frozen, i.e., weak Taylor's velocity), respectively. Space and time axes are scaled in arbitrary units according to u^* so that the Lagrangian ACF is along the identity line.

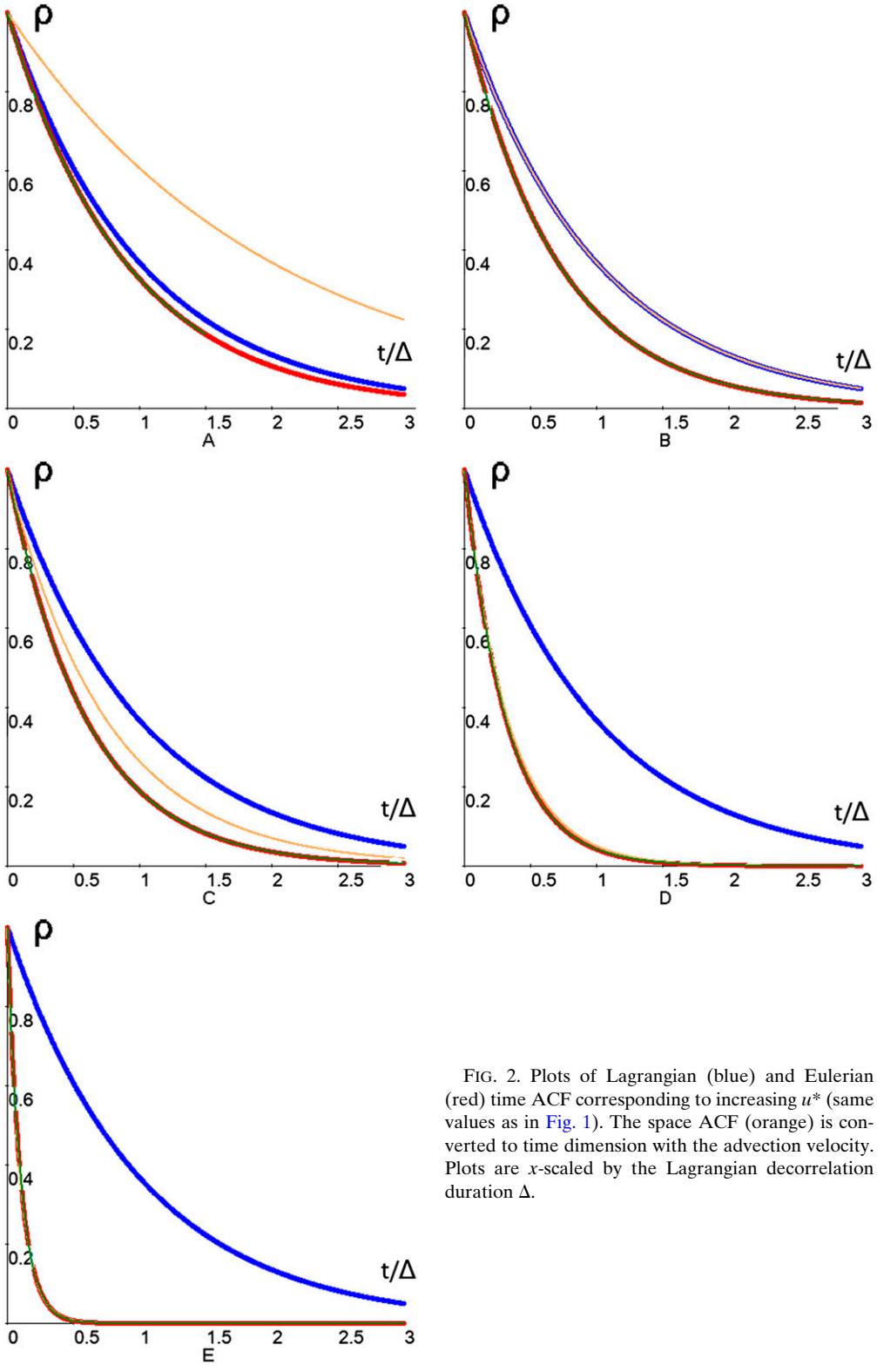

FIG. 2. Plots of Lagrangian (blue) and Eulerian (red) time ACF corresponding to increasing u^* (same values as in Fig. 1). The space ACF (orange) is converted to time dimension with the advection velocity. Plots are x-scaled by the Lagrangian decorrelation duration Δ.

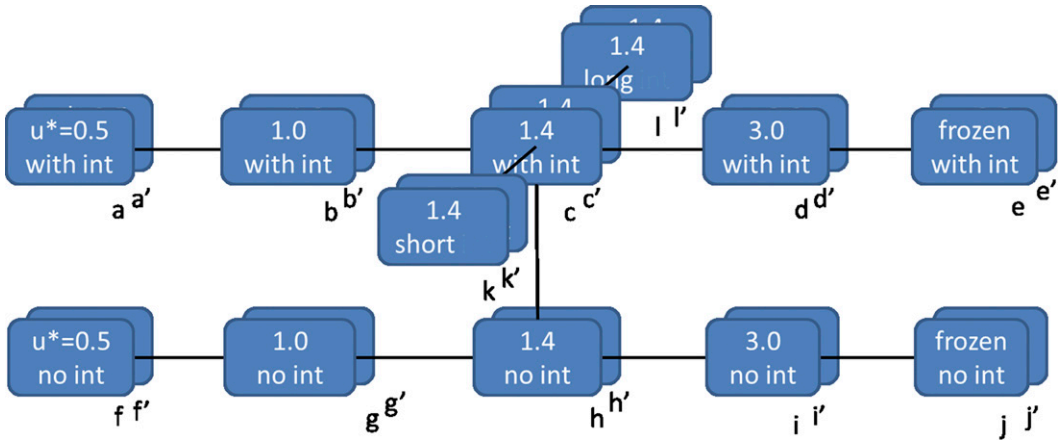

FIG. 3. Description of the 12 simulation experiments exploring increasing u^* velocity ratio values (ranging from 0.5 to 3.0 and frozen) under continuous (no int) and intermittent (with int) rainfall conditions. The central experiment (denoted c) mimics the original case study by Zawadzki (1973) over a 100-km range domain. For each experiment, the advection velocity is either assumed to be known and equal to the true parameter value (main frame with no prime notations) or assessed from the simulated fields (shadow frame with prime notation). The range of the study domain varies (k and l). Links indicate lines of changing parameter influence discussed in the paper.

rainfall intensity distribution, the intermittency of rainfall fields, the identification of the advection velocity, and various sampling effects. These difficulties are hard to formalize analytically. In the following, we use a numerical simulation to explore the respective importance of some of these difficulties in a range of fluctuations that mimics experimental conditions met in previous studies.

4. Model and parameters used for the numerical experiment

SAMPO (Leblois and Creutin 2013) is a stochastic rainfall simulator that adapts a classical Gaussian field simulation technique, the turning-band method, to produce sequences of rainfall fields satisfying three key features of actual precipitation systems: (i) the skewed distribution function at a point and the space–time structure of nonzero rainfall (NZR), (ii) the average probability and the space–time structure of rainfall intermittency, and (iii) a prescribed advection field.

The presented numerical study is centered on the experiment presented by Zawadzki (1973)—a summer midlatitude mesoscale convective system in Canada with a marked advection velocity. The advection velocity is taken equal to $18\,\mathrm{m\,s^{-1}}$ and is arbitrarily oriented toward the east. This linear advection is common to both intermittency (when present) and NZR fields that are nevertheless supposed to have distinct statistical features: specific mean and variance as well as specific space and time characteristic dimensions Λ and Δ, that is, specific Taylor's velocity. Having no specification about the distribution of the rainfall intensities at the elemental time step of simulation, we chose to keep the inverse-Gaussian distribution as in Leblois and Creutin (2013) without expected loss of generality. The NZR characteristics specified below correspond to natural rainfall intensities. The mean and standard deviation of NZR are 2.9 and $5.6\,\mathrm{mm\,h^{-1}}$, respectively, close to the maximum values given by Zawadzki (1973, his Fig. 8). The distance corresponding to a correlation in rain of $1/e$ is taken about 40 km in agreement with the space ACF plots given in his Figs. 12 and 13. The ratio u^* is 1.4 according to the ratio between the Lagrangian and Eulerian time characteristics (44 and 32 min at $1/e$), shown by his Fig. 10, remembering from Eq. (10) that this ratio equals $\sqrt{1+u^{*2}}$. For intermittency, a probability to have rain of 72% is retained from percentages of rain area fluctuating from almost 0% to ~80% during the active part of the event (his Fig. 8). The characteristic dimension of intermittency is 41 km, in agreement with the number of rainy areas present on the pictures of his Fig. 4 (~6–8 rain clusters in the radar scope at the highest activity).

As summarized in Fig. 3, the present sensitivity study relies on 24 experiments exploring various levels of "freezing" (u^* variation) under continuous or intermittent rainfall conditions and around the simulation of the original case study (denoted c′) of Zawadzki (1973). In each experiment, the advection velocity used to convert space to time ACF is either assessed from the simulated fields (prime notation) or assumed to be known and equal to the true parameter value (no prime notation). Each experiment consists of 400 storm period simulations over 8.5 h, that is, 33 time steps of 16 min.

The range of velocity ratios u^* considered includes basically the same values as in section 3 [$u^* = 0.5$, 1.0, and 3.0, plus $u^* = 1.4$ as in the case of Zawadzki (1973) and $u^* = 10^{30}$, an arbitrary large value for the frozen case]. The variety of tropical storms of the Amazon region, presented in Poveda and Zuluaga (2005), may be covered by the above range. We argue that the velocity ratio, more than the absolute values of the Taylor and advection velocities, governs the ACF signature.

The SAMPO model assumes the stationarity of the rainfall process in space and time. This assumption is behind many empirical analyses even if, as specified by Zawadzki (1973), the ACF analysis can be thought of in a more deterministic framework that geostatisticians name the transitive theory (Matheron 1965). For the purpose of this numerical study, this difference is not really relevant. We will consider that our results apply to a homogeneous period in a storm from which we determined the simulation parameters.

5. Advection velocity assessment

The advection velocity is estimated looking for the displacement $\mathbf{a}_0$ that maximizes the Eulerian ACF $A^E(\mathbf{a}_0, t_1 - t_2)$ over the time interval $t_1 - t_2$, which is the classical tracking radar echoes by correlation (TREC) method (Austin and Bellon 1974; Laroche and Zawadski 1995; and references therein). An iterative estimation at increasing grid resolution, close to the scaling-guess procedure of Laroche and Zawadzki (1995), drastically reduces the processing time.

In theory, the accuracy of assessment of the advection velocity depends on the space–time volume and shape of the storm compared to the size of the domain of observation D_s and to the sampling resolution characterized in time by Δt and space by Δx. The space–time volume of a storm is obtained by space–time integration of the function A^E and is equal to $8\pi\Lambda^2\Delta$ (Lantuéjoul 2002, appendix, Table 2). We will keep in mind its proportionality to Λ^2 and Δ and its independence on the advection velocity $\|\mathbf{U}\|$. Assessing the advection velocity needs both the surface of the storm to be smaller than the domain size and the volume of the storm to be much bigger than the space–time resolution. The space–time shape of a storm can be assessed by the length of its track at ground that is the fraction of its length Λ represented by its displacement $\Delta\|\mathbf{U}\|$. This fraction reads $\Delta\|\mathbf{U}\|/\Lambda$ that turns out to be u^*. The more the field is frozen and the more the storm has an elongated shape, the easier it is to analyze in terms of velocity direction. This is well analyzed in Poveda and Zuluaga (2005).

In practice, the present simulation uses a domain size of $200 \times 200\,\text{km}^2$ over 8.5 h. According to our reference case, only a range of 100 km around the domain center is considered to mimic radar coverage, and the sampling parameters are $\Delta x = 1$ km and $\Delta t = 16$ min. The variable Λ is taken as constant (41 km) and Δ takes five key values according to u^* (19, 38, 52, 114, and $\sim 10^{31}$ min when u^* is 0.5, 1.0, 1.4, 3.0, and 10^{30}). The observation volume covers the simulated storms well. The expected storm surface is one-fourth of the domain size and its volume is a tiny fraction of the observation volume (3.5%–7.5%—neglecting the reduction of the volume needed to cope with edge effects and advection that essentially reduces the length of efficient observation by the expected length of the storm track $\Delta\|\mathbf{U}\|$). The observation resolution is fine in space but, for low u^*, the time resolution gets too close to the characteristic time of the storm (16 and 19 min, respectively).

Figure 4 shows the advection velocities estimated for 400 simulated storm events over the basic set of velocity ratios u^*. The dispersion of the obtained results is isotropic and decreases when u^* increases, that is, when the advection velocity becomes relatively high compared to when Taylor's velocity is low or when the storm shape elongates.

As recapitulated in Fig. 5a, this dispersion increase is only marginally linked to the intermittency of the precipitation system. One can simply note that intermittency helps tracking when u^* is small. Figure 5b shows that the domain size given the resolution plays a less dominant role.

The case of Zawadzki (1973), close to the midsimulation case, looks at a case with low dispersion of the assessed advection velocity and direction in spite of its distance from the ideal frozen case. Most storm cases of Poveda and Zuluaga (2005) lay probably more toward the low u^* case, where the advection velocity is harder to identify, although the time resolution is different (7–10 min) and the characteristic time is quite constant (Eulerian ACF at $1/e$ around 30 min).

A more detailed sensitivity analysis exploring larger ranges of domain and resolution characteristics, using more sophisticated tracking methods and more complicated advection fields like in Germann and Zawadzki (2002), is achievable using SAMPO but is beyond the scope of this paper. The above short analysis is a simple illustration of the uncertainty of advection identification, remembering that this parameter governs the ACF signatures used to test Taylor's frozen hypothesis.

6. Testing Taylor's frozen hypothesis in continuous rainfall fields

In this section, we start testing the a priori favorable case of frozen fields by design ($u^* = 10^{30}$), and we next examine the effect of relaxing the frozen property of simulated

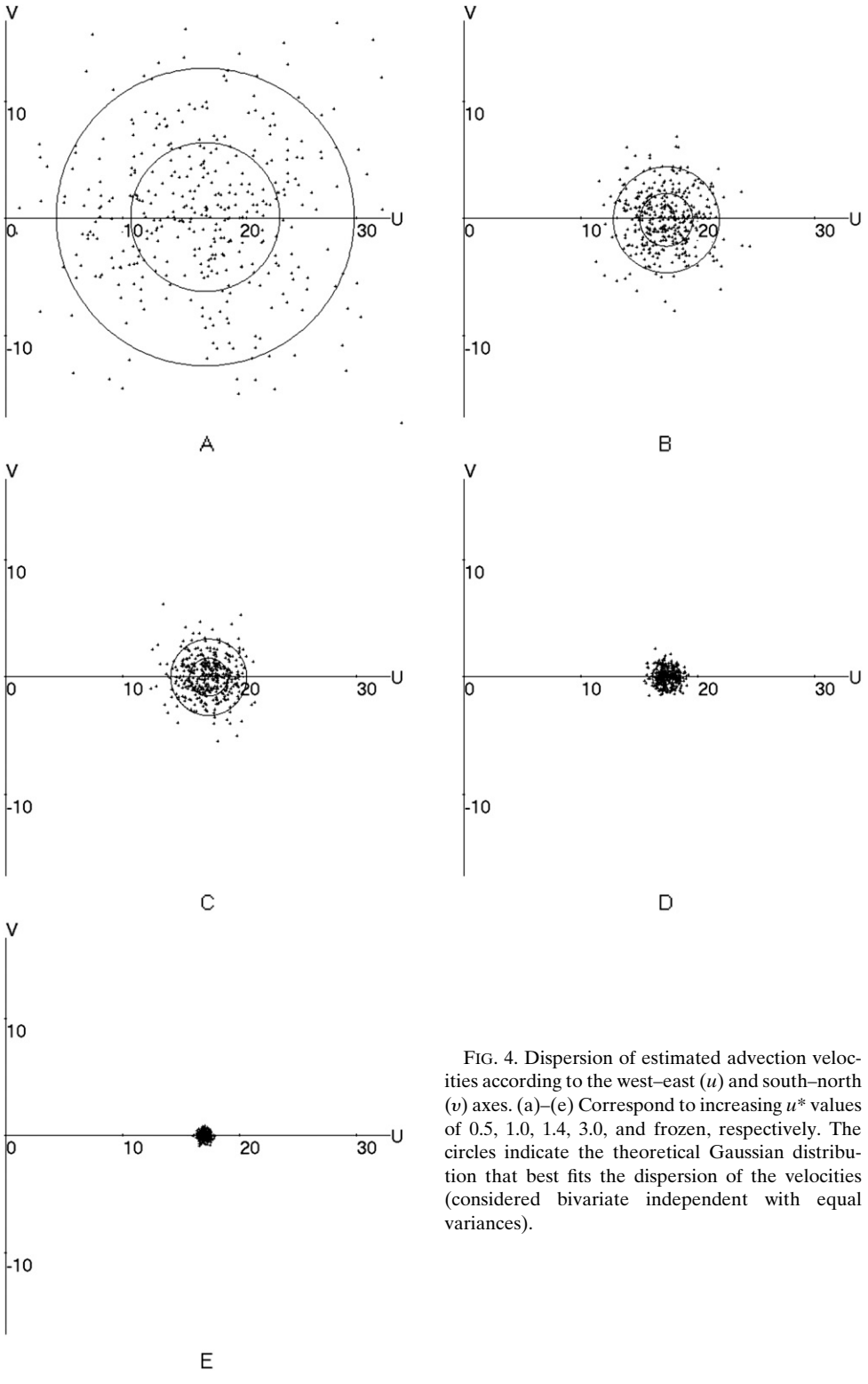

FIG. 4. Dispersion of estimated advection velocities according to the west–east (u) and south–north (v) axes. (a)–(e) Correspond to increasing u^* values of 0.5, 1.0, 1.4, 3.0, and frozen, respectively. The circles indicate the theoretical Gaussian distribution that best fits the dispersion of the velocities (considered bivariate independent with equal variances).

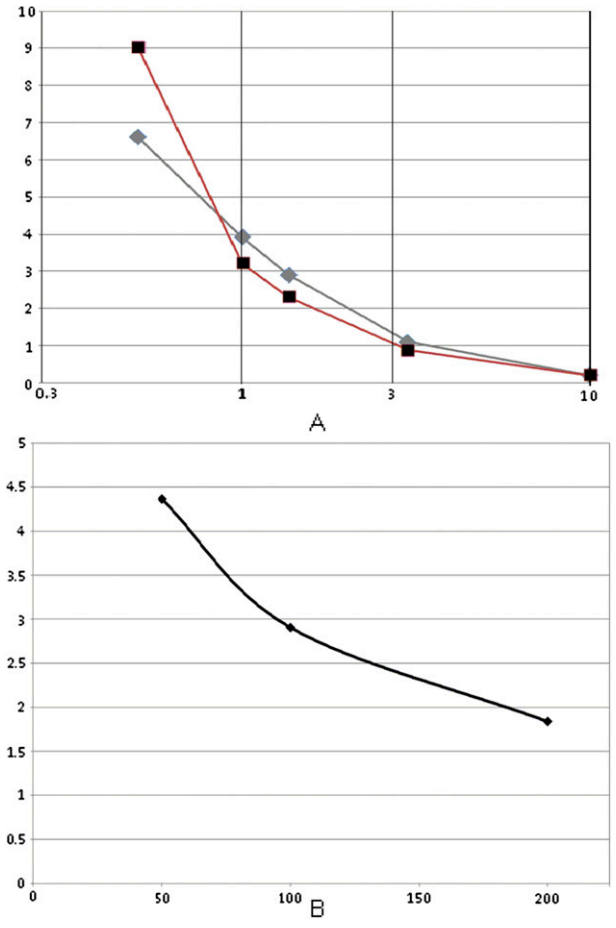

FIG. 5. Evolution of the advection uncertainty with (a) u^* and (b) the domain size. In both, the uncertainty is given as the RMSE ($m\,s^{-1}$) of the estimated advection velocity. In (a), u^* varies as in Fig. 4 in the presence (diamonds) or absence (squares) of intermittency. In (b), the domain radius varies from 50 to 200 km.

fields by taking decreasing values of u^* [simulations f–j of Fig. 3, denoted SIM(f–j)]. In both experiments, we consider that there is no intermittency and that advection velocity is known. We thus eliminate fluctuations due to imperfect space–time anisotropy, intermittency, or advection velocity assessment. The simulation allows us to consider both individual event results and their ensemble features. We illustrate the capability of the ACF signature to test the frozen hypothesis using two types of representation. The first one, like in Fig. 6, displays the ensemble of event ACF signatures and their mean and standard deviation. The second one relies on the conversion factor $\hat{\mathbf{U}}^E$ best suited to match, event per event, Eulerian time and space ACFs at short distance (minimization of the squared differences between the two functions up to the decorrelation distance of $1/e$, i.e., six values in our case). It shows, like in Fig. 7, the empirical cumulative distribution function (CDF) of the ratio $\hat{\mathbf{U}}^E/\mathbf{U}$ that measures the adequacy of the advection velocity $\mathbf{U}$ to produce a good fit and thus to validate the hypothesis. In our model, the theoretical value of this ratio is given by $u^*/\sqrt{1+u^{*2}}$ and is shown with the empirical CDF. Below we use the term "adequacy CDF."

Figures 6 and 7 are about the simulation of frozen fields [SIM(j)]. In Fig. 6, the two beams of simulated Eulerian time- and space-converted ACFs overlap well and the average values are almost perfectly equal over the complete range. The Lagrangian time ACF looks far from what we expect from the frozen hypothesis: the dispersion is considerable and the average behavior is slightly biased compared to the expected constant value. The slightly larger dispersion of the space ACF suggests some more sampling dispersion in identifying space than time structure. Figure 7 gives a more specific look at the event per event match between the time- and space-converted Eulerian ACFs, that is, for the event per event ability, we have to check the frozen hypothesis through the classical use of the ACF signature. On average, the frozen hypothesis is positively tested given the perfect symmetry of the experimental adequacy CDF in regard to the axis 1. This is expected from the chosen u^* in our simulation and confirmed by the theoretical adequacy value that is confounded with this axis. Considering its dispersion, this CDF roughly indicates a 0.5 probability to have a mismatch between the ACFs greater than 20% when using the known advection velocity to check the hypothesis. The dispersion in general, as well as the difference between the Lagrangian average and the expected theoretical constant, is due to the limited support of the simulated fields. Our first conclusion is that, in front of a perfect frozen event, the classical way to test the frozen hypothesis works well on average but may be difficult to analyze event per event given the demonstrated dispersion.

Figures 8 and 9 are about SIM(f–j), when taking a range of u^*. Figure 8 shows an evolution of the average ACF signature that is quite consistent with the analytical exercise shown in Fig. 2. The respective positioning of the different ACF evolves the same way when u^* increases, including the steady movement of the Lagrangian toward the Eulerian ACF, away from a perfect correlation $A(0,0)$. If we consider the event dispersion, a salient point is that the overlap between the Eulerian and the converted space ACF beams persists even with values of u^* being less than 1. This point is quite consistent with the CDF representation of Fig. 9, where we have typically three behaviors. When $u^* > 3$, we remain basically in the frozen situation like in Fig. 7. When $1 < u^* < 3$, the CDF starts to shift significantly toward values lower than 1 in good agreement with the average value predicted by the model. The dispersion does not

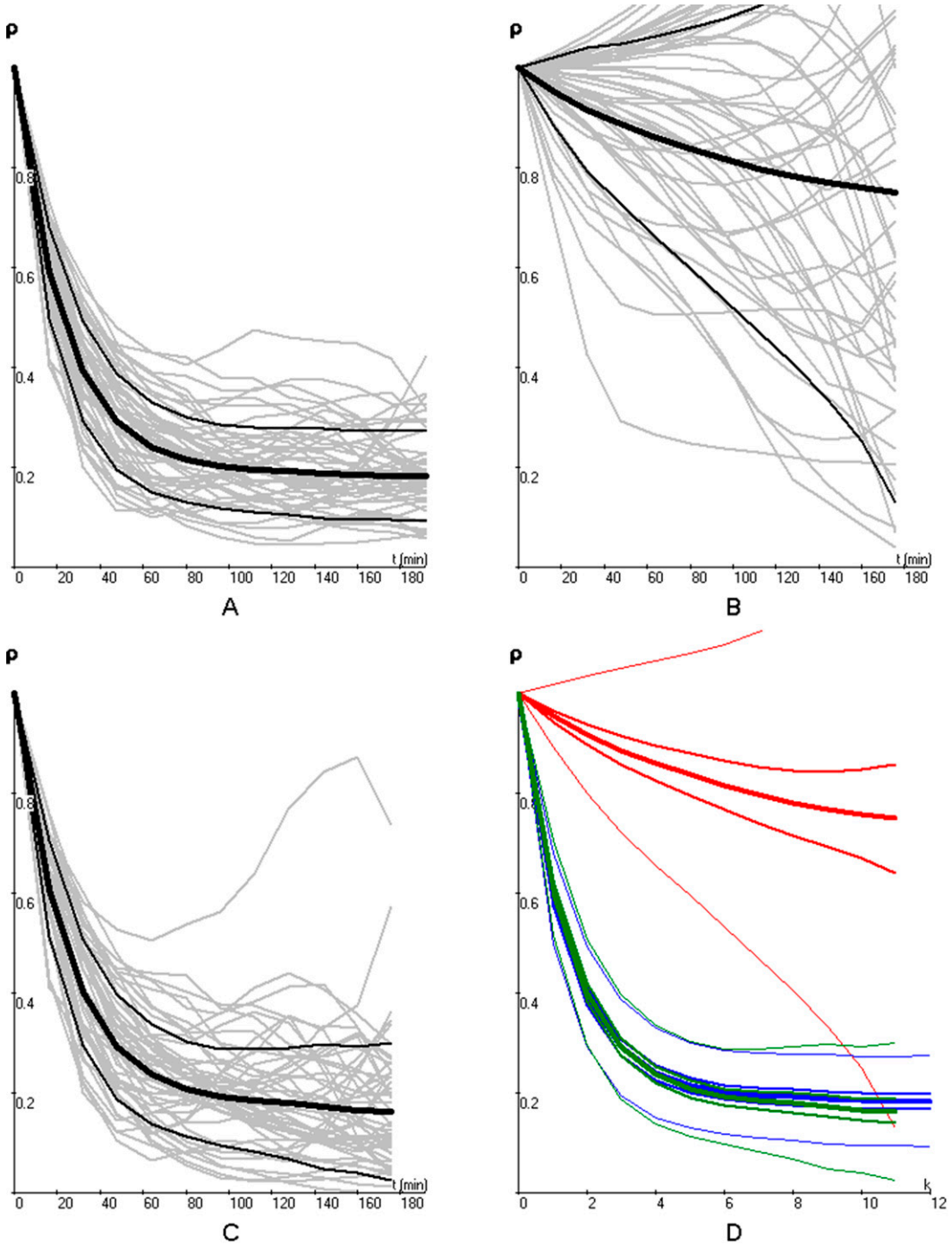

FIG. 6. ACF signature for 400 events as close as possible to frozen ($u^* = \sim 10^{30}$). (a) Eulerian time ACF, (b) Lagrangian time ACF, and (c) space–time ACF converted through the prescribed advection velocity value are represented separately in order to display the dispersion of the individual event ACF (gray) and the average simulated value (black; thick for the mean and thin for the std dev). For readability, ACFs for only 50 events are displayed. (d) The three average ACFs and their confidence interval (Lagrangian in red, Eulerian in green, and converted space in blue).

increase notably. When $u^* < 1$, both the shift and the dispersion increase dramatically and even the predicted average value turns out to be contradicted by the simulated values, indicating finally too big of a gap between the hypothesis and the model properties. Note that, even when u^* is below 1, the CDF cuts the 1 axis, leaving almost 30% of the obtained values reasonably close to 1 and diagnosing positively the frozen

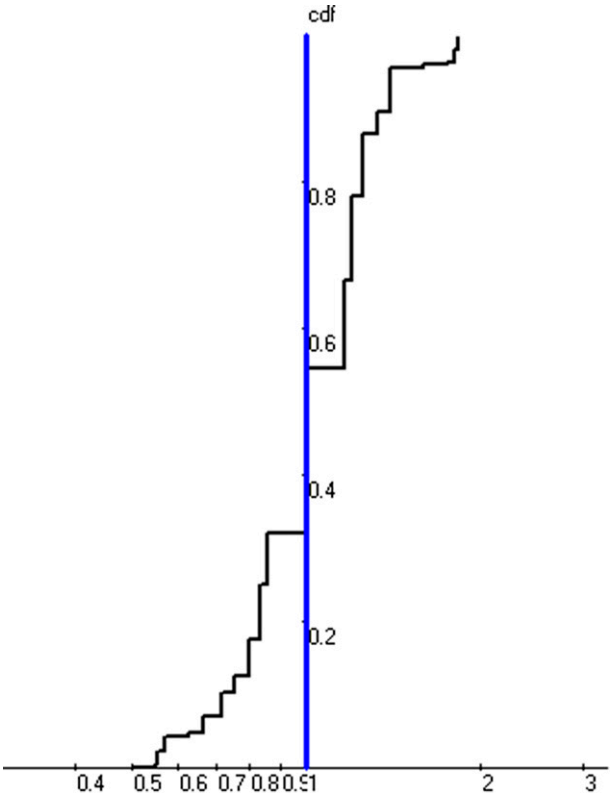

FIG. 7. Empirical adequacy CDF for the same frozen experiment as in Fig. 6. The blue line is the theoretical value of the adequacy ratio.

hypothesis. Our second conclusion is that as long as advection velocity is larger than Taylor's velocity ($u^* > 1$), the classical test of the frozen hypothesis responds positively in a majority of cases.

Figure 10 shows that the dispersion of the Lagrangian ACF of individual events increases with u^*. The distance between Eulerian and Lagrangian ACFs thus appears, on average and in dispersion, more selective than the classical criterion using the converted space ACF. Our third conclusion is that the Lagrangian ACF is very useful to appreciate the validity of the frozen hypothesis. We thus recommend taking a comprehensive view of the ACF signature, including the Lagrangian one, to test the frozen hypothesis.

7. Sensitivity to advection assessment, intermittency, and domain size

The validation of the frozen hypothesis using the ACF signature can be sensitive, among other factors, to (i) the accuracy of the advection velocity used to convert ACFs from space to time [SIM(f–j) vs SIM(f′–j′)] and (ii) the presence of intermittency in the precipitation fields [SIM(a–e) vs SIM(f–j)].

Figure 11 shows a modest effect of advection assessment on the converted space ACF and its dispersion. The dispersion raise when using estimated instead of prescribed advection velocities is more significant at short distances and when u^* is weak, as expected from the accuracy of the advection velocity assessment seen in Fig. 3. This effect is easier to interpret in Fig. 12, where the CDFs for $u^* = 0.5$ show that uncertainty on advection velocity leads to a much larger number of failures of the diagnostic. When the advection is assessed, the CDF cuts the 1 axis around 0.8 with a slope allowing still 20%–30% of the ratios reasonably close to 1. Our conclusion is that the need to assess advection velocity further degrades the diagnosing capacity of the classical test of the frozen hypothesis.

We finally apply the same test to bulk rainfall fields, that is, intermittent fields for which ACFs are computed with both zero and nonzero rainfall values. Figure 13 shows the signature of the pivoting case of Zawadzki (1973) without and with intermittency. The presence of intermittency changes the range of the ACFs that decreases by typically 30%, a ''mechanical'' effect due to the change of variance of the rainfall field, but the ACF signature and the associated sampling dispersion remain quite close. The ACF signature appears also to be insensitive to the characteristic dimension (or decorrelation length) of the intermittency (test not shown here). The relative size of the domain to the characteristic length of the intermittency has a great influence on the estimation of the adequacy factor. As shown in Fig. 14, when the size of the considered domain increases, passing from ~2 to 10 times the characteristic length of the intermittency (40 km), the average adequacy factor decreases, moving toward its theoretical value. Its dispersion also decreases notably. Both results confirm the influence of the domain size, putting a single radar scope at the lower size limit. Our conclusion is that rainfall intermittency does not disturb the test of the frozen hypothesis, provided the covered domain is large enough, which seems to be the case of standard weather radar coverage.

8. Conclusions

Paraphrasing Gupta and Waymire (1987), we can say today that the geometry and kinematics of rain fields have been the subject of constant interest over the last four decades, that is, since the seminal works of Austin and Houze (1972) and Zawadzki (1973). In this line of research, the hypothesis of frozen turbulence, proposed by Taylor (1938) as a very convenient way to relate the space and time variability, played an important role in frameworks as varied as classical space–time models or fractal or cascade models.

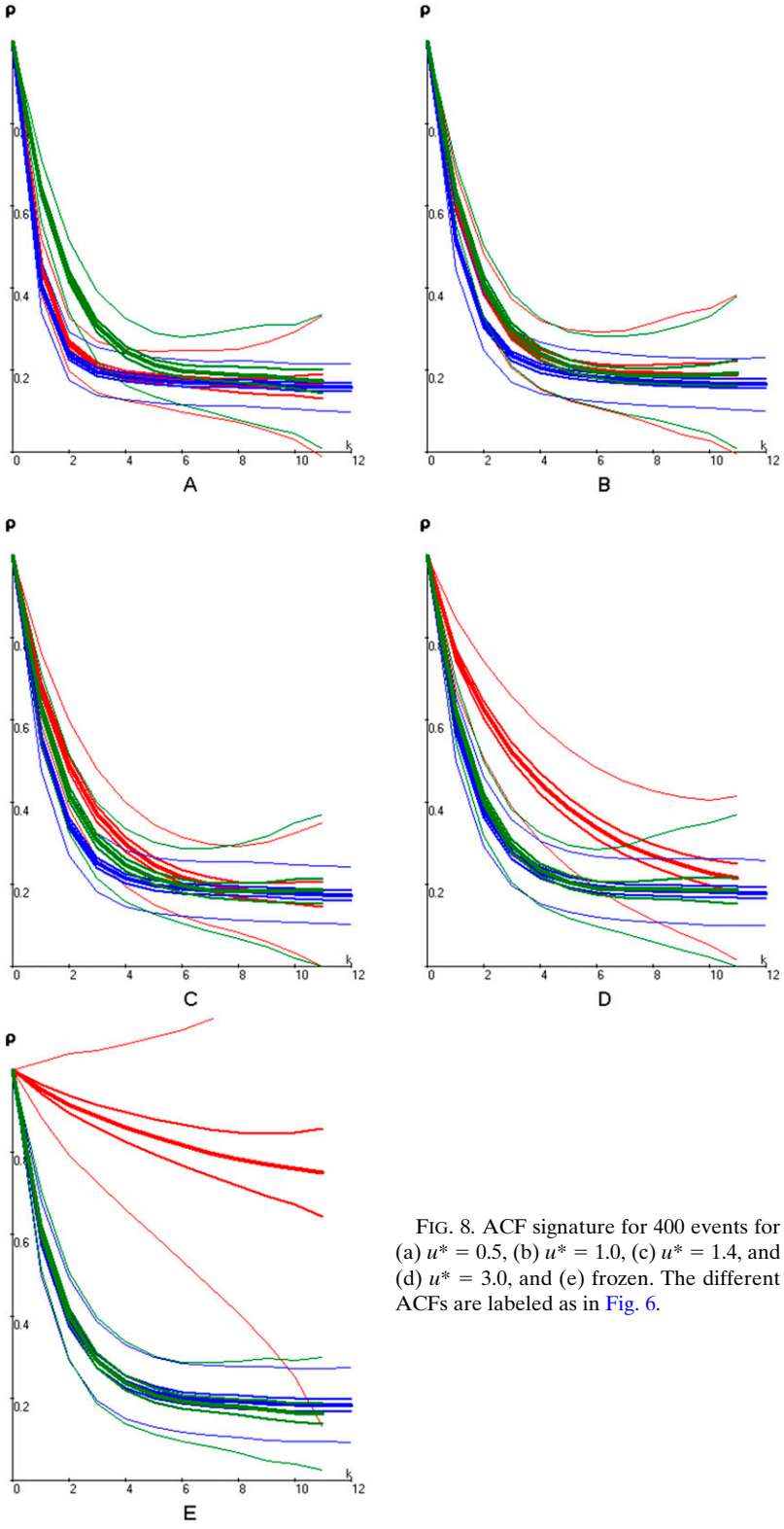

FIG. 8. ACF signature for 400 events for (a) $u^* = 0.5$, (b) $u^* = 1.0$, (c) $u^* = 1.4$, and (d) $u^* = 3.0$, and (e) frozen. The different ACFs are labeled as in Fig. 6.

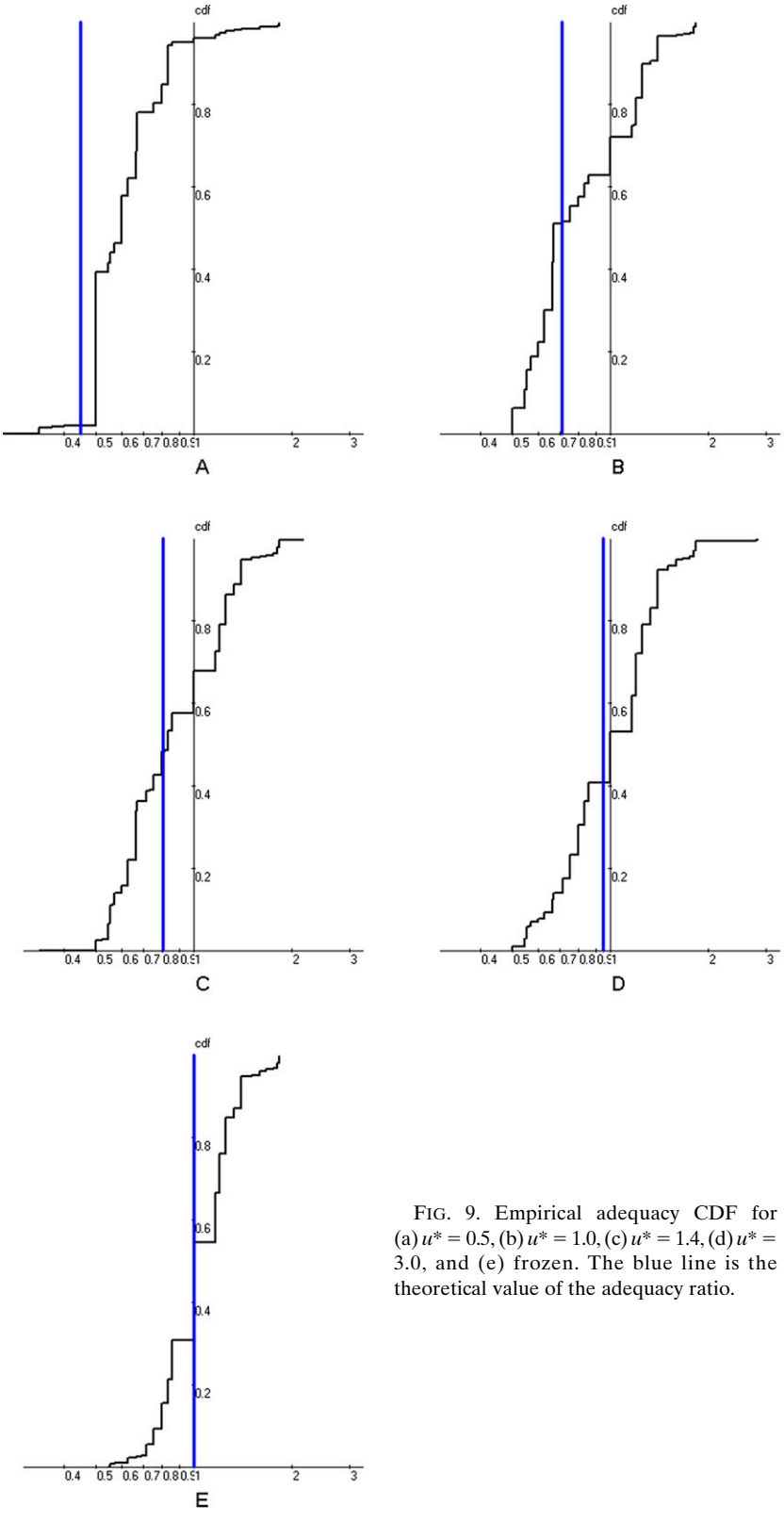

FIG. 9. Empirical adequacy CDF for (a) $u^* = 0.5$, (b) $u^* = 1.0$, (c) $u^* = 1.4$, (d) $u^* = 3.0$, and (e) frozen. The blue line is the theoretical value of the adequacy ratio.

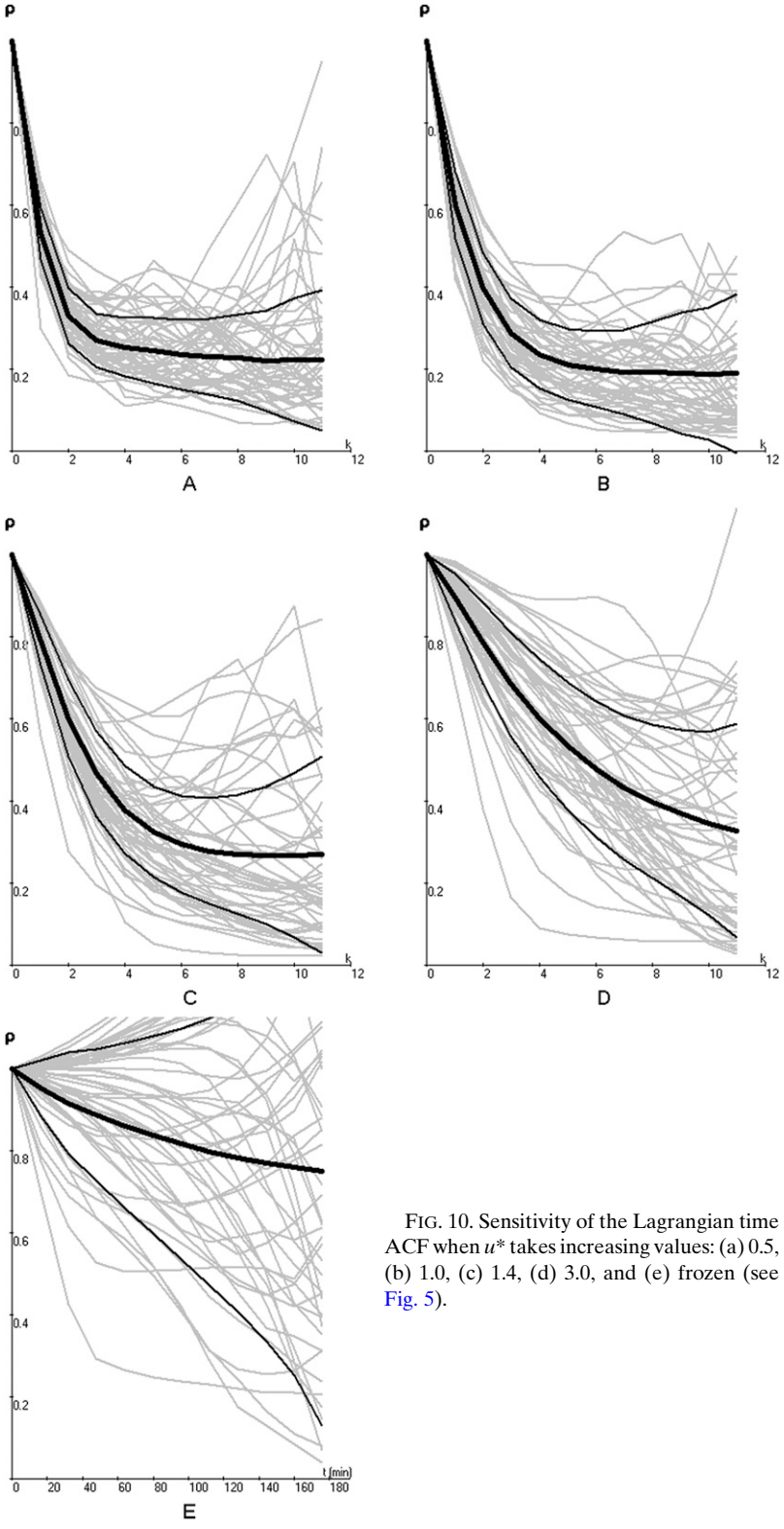

FIG. 10. Sensitivity of the Lagrangian time ACF when u^* takes increasing values: (a) 0.5, (b) 1.0, (c) 1.4, (d) 3.0, and (e) frozen (see Fig. 5).

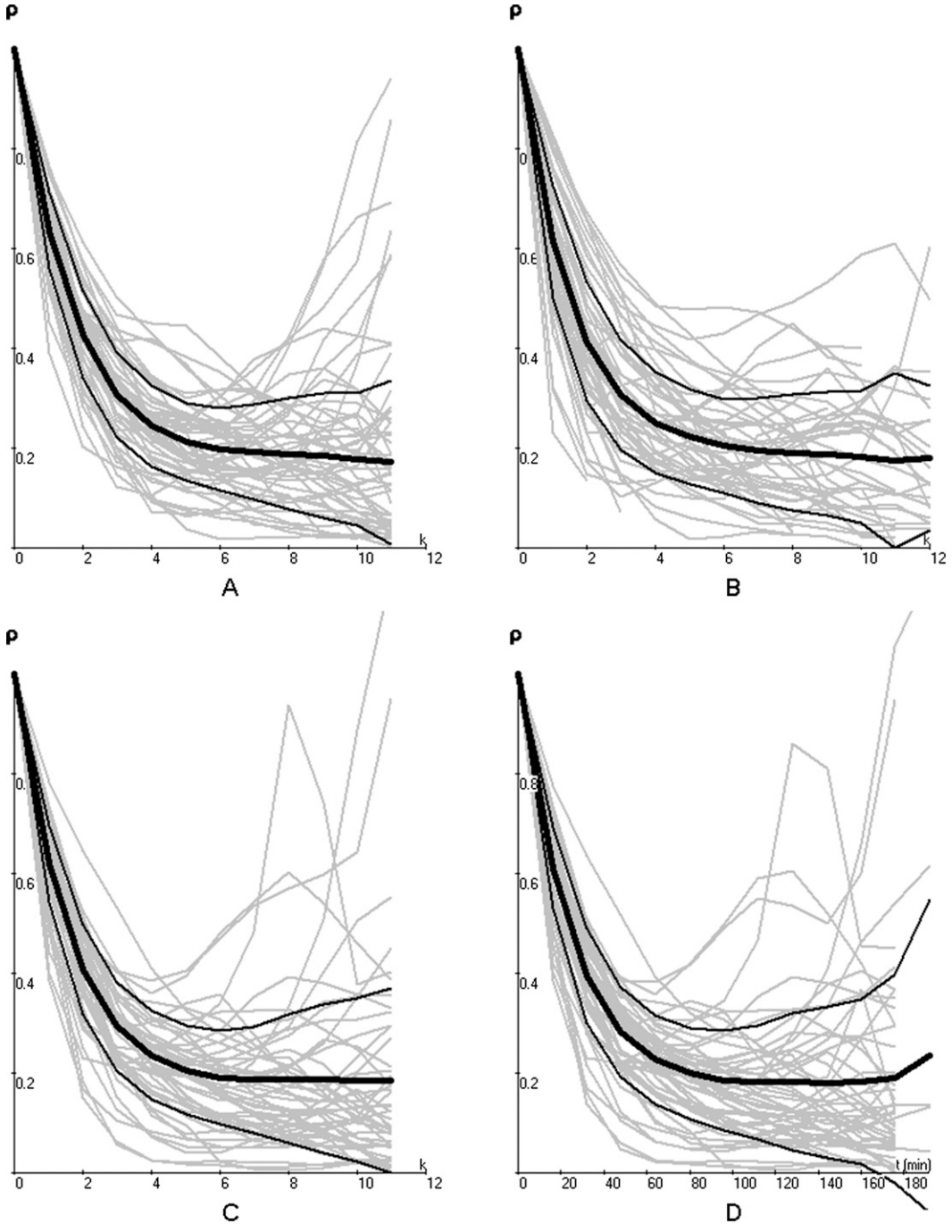

FIG. 11. Space ACF converted using the (left) prescribed advection velocity and (right) assessed advection velocity when (a),(b) $u^* = 0.5$ and (c),(d) $u^* = 3.0$.

At the end of this study, our conclusion is twofold. Taylor's hypothesis, understood as the quest of a space–time symmetry in rain field variability, remains important in hydrometeorology. The so-called frozen hypothesis, introduced for simplification purposes, appears difficult to check and unnecessarily constraining.

Taylor's approach invites one to distinguish large- and small-scale variability and to assume that the statistical properties related to the time dimension relate to those in the space dimension through a simple linear coordinate transformation. These properties are those of the geostatistical model used in this study and are common to

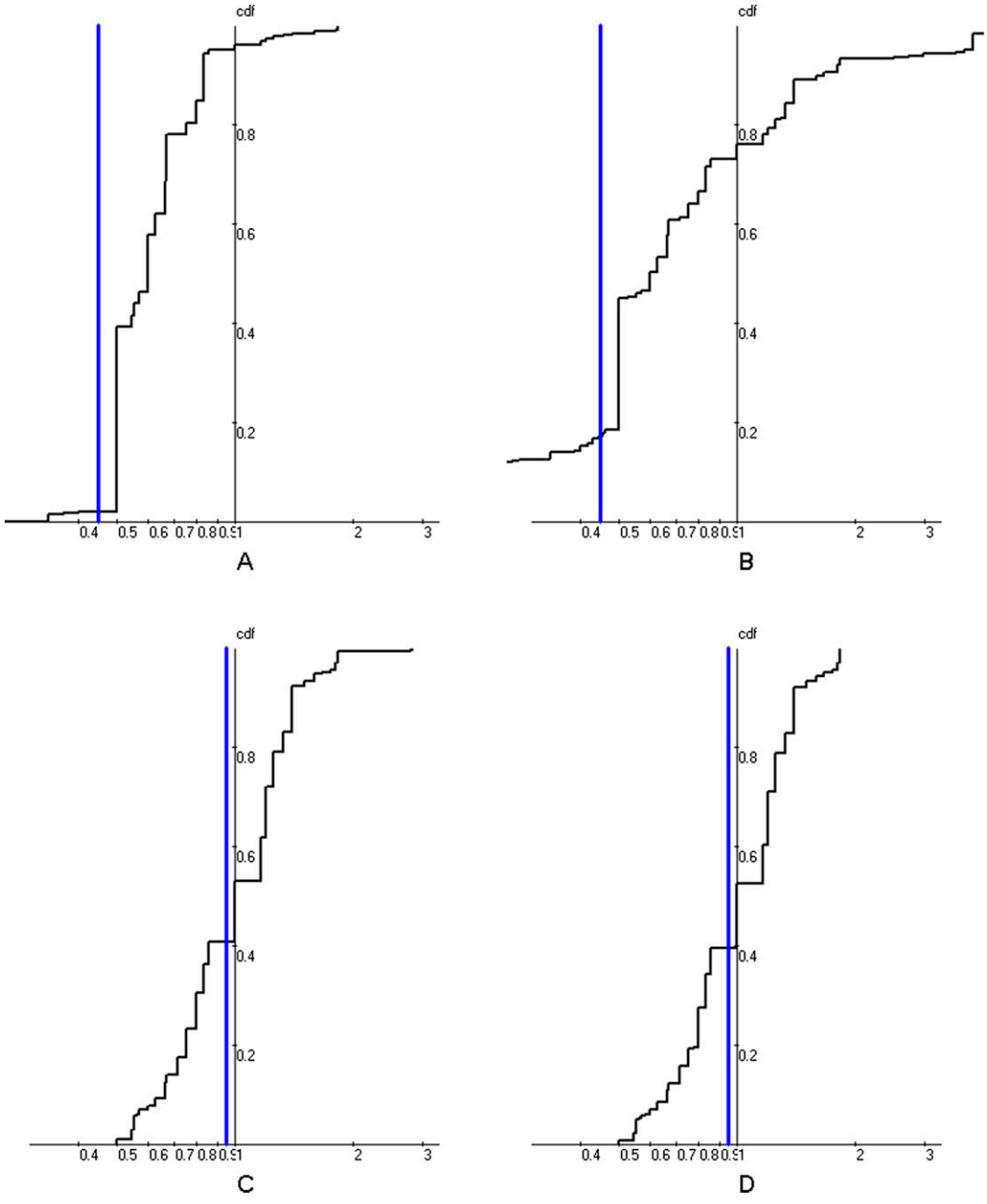

FIG. 12. Empirical adequacy CDF using the (left) prescribed advection velocity and (right) assessed advection velocity when (a),(b) $u^* = 0.5$ and (c),(d) $u^* = 3.0$.

most state-of-the-art rainfall stochastic models. They allow us to reproduce the consensual distinction between advection and intrinsic variability of rainfall in a parsimonious model setting and to make use of the many mathematical techniques producing isotropic 3D fields to be used in hydrometeorology. Rainfall stochastic modeling remains of interest for theoretically linking the Lagrangian and Eulerian rainfall variability and, in turn, for interpreting gauge patrimonial data that remain of interest for climatological studies in spite of recent progress in radar detection.

The frozen hypothesis appears to be very difficult to check. Our analytical developments attract attention on at least three recommendations about the classical use of the ACF signature as a test of the frozen hypothesis. The first is when u^* is close to 1, that is, when the two characteristic velocities are equal. In this case, the mere superposition of the converted space ACF and the

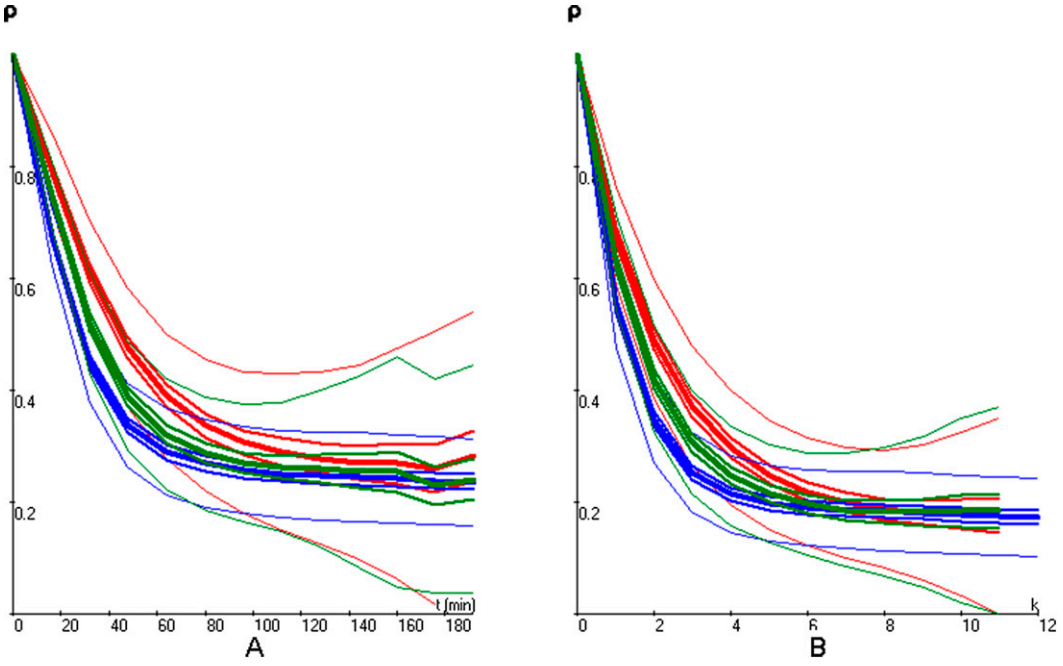

FIG. 13. ACF signatures for 400 events for the velocity ratio $u^* = 1.4$ in (a) absence or (b) presence of intermittency. ACFs are labeled as in Fig. 6.

Eulerian time ACF may be good for wrong reasons. The second is that the Lagrangian time ACF should not be ignored as a quite robust and sensitive indicator of the distance to the frozen case. The third is that the ACF signature is graphically operative only within the range $0.4 < u^* < 2.5$. As far as we understand, Zawadzki (1973) was in the case of ambiguity when the characteristic velocity is unique or when the advection velocity is the good conversion velocity (agreement of the ACF) for the wrong reason (Lagrangian ACF far from being constant). Li et al. (2009), focusing only on the distance between the converted space ACF and the Eulerian time ACF [their Eq. (2)], may have several cases in their analysis that are wrongly diagnosed as frozen. Our numerical simulations invite one to exercise caution about how the sampling dispersion of individual ACF signatures makes the event by event analysis difficult. Because of the dispersion of estimations, we do not believe an event-based analysis can be enough to detect a cutoff time, that is, a lag beyond which the converted spatial

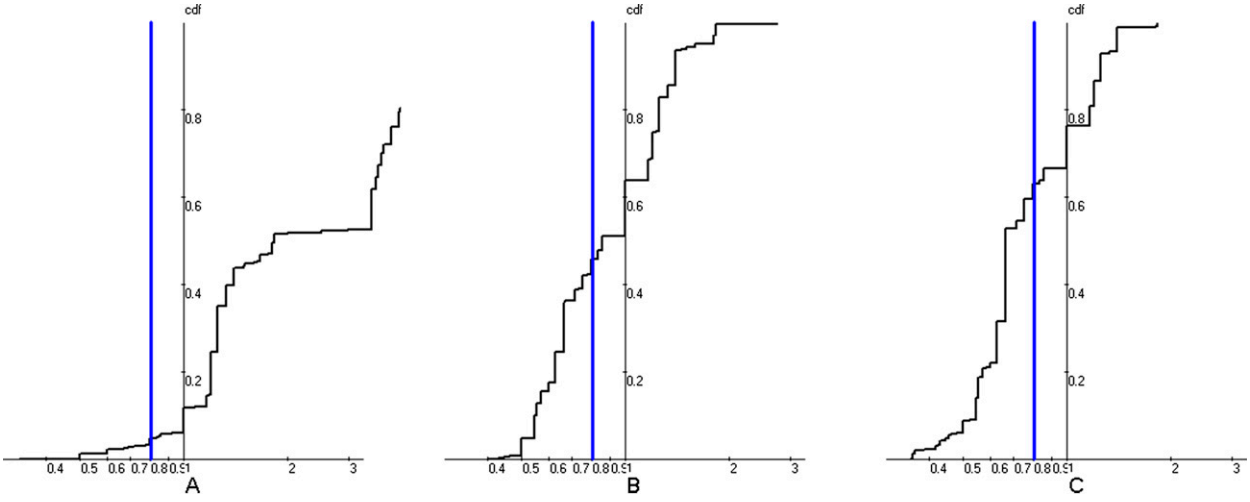

FIG. 14. Empirical adequacy CDF when $u^* = 1.4$ and over domains of increasing size: radius of (a) 50, (b) 100 (reference), and (c) 200 km.

ACF and the Eulerian time ACF would diverge. Among the various sources of dispersion explored in this study, no one appeared to be significantly dominant beyond the fact that the value of u^* directly governs the degree of freezing detected by the ACF signature, a property by design. The frozen hypothesis appears overall too constraining regarding practical and more methodological considerations.

In practice, all the ACF signatures seen in the literature look far from the frozen case, at least considering the most probing Lagrangian time ACF. Our study proposes using two characteristic velocities instead of one, and for this we recommend using only the Lagrangian and Eulerian time ACFs as the ACF signature. The slope ratio between Lagrangian and Eulerian ACFs gives access to u^* through Eq. (4), and the position of the time Lagrangian ACF compared to a constant value $A(0, 0)$ eventually indicates a frozen case.

From a methodological point of view, freezing the small-scale variability wipes out the multiscale nature of Taylor's approach included in SAMPO. Using two characteristic velocities, that is, ''unfreezing'' Taylor's hypothesis, allows us to distinguish two levels of precipitation variability: (i) a global level governed by the ''visible'' movement of precipitation, the advection velocity, which is responsible for the time asymmetry of the ACF, and (ii) a local level representing the precipitation dynamics at lower scales, the Taylor's velocity, which is responsible for the space–time anisotropy of the ACF. Using more than one Taylor's velocity allows is to represent additional levels of local-scale variability by simply summing independent processes having different characteristic scales and dynamics. It is in this sense that unfreezing Taylor's hypothesis allows us to better capture the multilevel nature of precipitation.

As a side result, the simulations performed in this study show that the assessment of the advection velocity becomes difficult as soon as u^* becomes smaller than 1. Our analytical developments reveal the noticeable difference between the two methods classically used to assess the advection velocity. They show that the maximum cross correlation between nearby locations used for rain gauge networks (e.g., Niemczynowicz 1988; Crane 1990; Upton 2002) is biased compared to the maximum cross correlation between successive time steps used for radar data [the TREC method of Austin and Bellon (1974) or Laroche and Zawadzki (1995), for instance], the bias disappearing when u^* is high, that is, when the frozen hypothesis is satisfied.

The above elements of conclusion invite one to check some key experimental properties regarding advection; Taylor's velocity; and, more comprehensively, the ACF signature over a long-term radar dataset. Properties of U and U_T are the main things we would like to look in real data, so as to see if u^* changes at some point in actual situations. This needs a strategy to describe the variability of advection across scales.

Acknowledgments. The authors acknowledge the financial support of their host institutions CNRS, Irstea, and the Norwegian Meteorological Institute as well as from the French National Research Council (ANR-11-BS56-0027 Floodscale Project) and from the Norwegian foundation Sintef Energy (weather generator pilot project).

REFERENCES

Austin, G. L., and A. Bellon, 1974: The use of digital weather radar records for short-term precipitation forecasting. *Quart. J. Roy. Meteor. Soc.*, **100**, 658–664, doi:10.1002/qj.49710042612.

Austin, P. M., and R. A. Houze Jr., 1972: Analysis of the structure of precipitation patterns in New England. *J. Appl. Meteor.*, **11**, 926–935, doi:10.1175/1520-0450(1972)011<0926:AOTSOP>2.0.CO;2.

Bowler, N. E., C. E. Pierce, and A. Seed, 2004: Development of a precipitation nowcasting algorithm based upon optical flow techniques. *J. Hydrol.*, **288**, 74–91, doi:10.1016/j.jhydrol.2003.11.011.

Crane, R. K., 1990: Space–time structure of rain rate fields. *J. Geophys. Res.*, **95**, 2011–2020, doi:10.1029/JD095iD03p02011.

Fabry, F., 1996: On the determination of scale ranges for precipitation fields. *J. Geophys. Res.*, **101**, 12 819–12 826, doi:10.1029/96JD00718.

Germann, U., and I. Zawadzki, 2002: Scale-dependence of the predictability of precipitation from continental radar images. Part I: Description of the methodology. *Mon. Wea. Rev.*, **130**, 2859–2873, doi:10.1175/1520-0493(2002)130<2859:SDOTPO>2.0.CO;2.

Gupta, V. K., and E. Waymire, 1987: On Taylor's hypothesis and dissipation in rainfall. *J. Geophys. Res.*, **92**, 9657–9660, doi:10.1029/JD092iD08p09657.

Lantuéjoul, C., 2002: *Geostatistical Simulation: Models and Algorithms.* Springer, 256 pp.

Laroche, S., and I. Zawadzki, 1995: Retrievals of horizontal winds from single-Doppler clear-air data by methods of cross correlation and variational analysis. *J. Atmos. Oceanic Technol.*, **12**, 721–738, doi:10.1175/1520-0426(1995)012<0721:ROHWFS>2.0.CO;2.

Leblois, E., and J.-D. Creutin, 2013: Space–time simulation of intermittent rainfall with prescribed advection field: Adaptation of the turning band method. *Water Resour. Res.*, **49**, 3375–3387, doi:10.1002/wrcr.20190.

Li, B., A. Murthi, K. P. Bowman, G. R. North, M. G. Genton, and M. Sherman, 2009: Statistical tests of Taylor's hypothesis: An application to precipitation fields. *J. Hydrometeor.*, **10**, 254–265, doi:10.1175/2008JHM1009.1.

Lovejoy, S., and B. Mandelbrot, 1985: Fractal properties of rain, and a fractal model. *Tellus*, **37A**, 209–232, doi:10.1111/j.1600-0870.1985.tb00423.x.

Matheron, G., 1965: *Les variables régionalisées et leur estimation.* Masson, 305 pp.

Niemczynowicz, J., 1988: The rainfall movement—A valuable complement to short-term rainfall data. *J. Hydrol.*, **104**, 311–326, doi:10.1016/0022-1694(88)90172-2.

Poveda, G., and M. D. Zuluaga, 2005: Testing Taylor's hypothesis in Amazonian rainfall fields during the WETAMC/LBA

experiment. *Adv. Water Resour.*, **28**, 1230–1239, doi:10.1016/j.advwatres.2005.03.012.

Taylor, G. I., 1938: The spectrum of turbulence. *Proc. Roy. Soc. London*, **164**, 476–490, doi:10.1098/rspa.1938.0032.

Upton, G. J. G., 2002: A correlation–regression method for tracking rainstorms using rain-gauge data. *J. Hydrol.*, **261**, 60–73, doi:10.1016/S0022-1694(01)00618-7.

Waymire, E., V. K. Gupta, and I. Rodriguez-Iturbe, 1984: A spectral theory of rainfall intensity at the meso-β scale. *Water Resour. Res.*, **20**, 1453–1465, doi:10.1029/WR020i010p01453.

Wu, X., and M. Yanai, 1994: Effects of vertical wind shear on the cumulus transport of momentum: Observations and parameterization. *J. Atmos. Sci.*, **51**, 1640–1660, doi:10.1175/1520-0469(1994)051<1640:EOVWSO>2.0.CO;2.

Zawadzki, I., 1973: Statistical properties of precipitation patterns. *J. Appl. Meteor.*, **12**, 459–472, doi:10.1175/1520-0450(1973)012<0459:SPOPP>2.0.CO;2.

——, J. Morneau, and R. Laprise, 1994: Predictability of precipitation patterns: An operational approach. *J. Appl. Meteor.*, **33**, 1562–1571, doi:10.1175/1520-0450(1994)033<1562:POPPAO>2.0.CO;2.